Int. J. Heat Mass Transfer. Vol. 36, No. 13, pp. 3361–3367, 1993
Printed in Great Britain

0017–9310/93 $6.00+0.00

Natural convection in a vertical cylinder filled with anisotropic porous media

WEN-JENG CHANG and CHI-FENG HSIAO
Department of Mechanical Engineering, Feng Chia University, Taichung, Taiwan, R.O.C.

(*Received* 21 *August* 1992)

Abstract—A SIMPLE numerical algorithm is used to analyze the natural convection in a vertical cylindrical enclosure filled with a saturated anisotropic porous medium. The boundary conditions of the enclosure are assumed to be maintained at a uniform high temperature except that the temperature of the bottom is low. The effects of anisotropic permeability ratio, anisotropic thermal conductivity ratio, geometrical aspect ratio and Rayleigh number on the flow field and heat transfer are investigated. Numerical results show that the heat transfer rates of the side and bottom walls increase, either decreasing the values of anisotropic permeability ratio or increasing the values of anisotropic thermal conductivity ratio, and the side average Nusselt number increases as the aspect ratio decreases.

1. INTRODUCTION

NATURAL convection in saturated porous media has recently received considerable attention because of numerous applications. Such applications include natural convection in geothermal reservoirs, aquifers, porous insulations, packed bed reactors, sensible heat storage beds, and beds of fossil fuel such as oil shale and coal. Excellent reviews are available by Cheng [1, 2] and Combarnous [3]. The most common practice is to describe heat transfer in porous media, made up of a solid matrix and a saturated fluid, as a fictitious continuum.

The previous researchers primarily concerned one of the two extreme configurations in which the phenomenon could exist: (1) the fluid layer heated from the side, and (2) the fluid heated from below. The early experimental studies of Schneider [4] demonstrated that the net heat transfer across the porous layer increases monotonically as the Rayleigh number increases. The theoretical work on the convection-dominated regime of porous layers heated from the side was pioneered by Weber [5] who developed on Oseen-linearized solution for the boundary layer regime in a tall layer. Weber's solution was modified later by Bejan [6] to account for the heat transfer taking place vertically through the core region of a moderately tall layer. In addition, the articles by Peirotti *et al.* [7], Vasseur *et al.* [8], Poulikakes and Bejan [9], Prasad and Kulacki [10, 11] should be consulted, as should the study of the connective flow of fluid through porous media heated from below, from early studies by Horton and Rogers [12], through numerical studies by Wooding [13], Horne and O'Sullivan [14], to experimental studies by Combarnous and LeFur [15] and Caltagirone *et al.* [16].

So far, the investigations have usually been concerned with isotropic porous media. However, many porous materials are anisotropic, for example, fibrous insulation materials. Another important example is groundwater motion in sediments and other anisotropic rocks, especially in areas with geothermal activity. Kvernvold and Tyvand [17] performed the theoretical investigation of convective flows in horizontally anisotropic porous layers. Burns *et al.* [18] incorporated anisotropic permeability in their study of convection in vertical slots. Bories [19] studied the effect of anisotropy on the criterion for the onset of convection.

The purpose of the present work is to investigate the flow in an anisotropic porous medium due to buoyancy in a vertical cylindrical enclosure in which the temperature (T_h) of the top and circumferential surfaces of the enclosure are the same and higher than that of the bottom wall (T_c), for a wide range of parameters: $0.1 \leqslant K^* \leqslant 10$, $0.1 \leqslant \lambda \leqslant 10$, $0.5 \leqslant A \leqslant 2$ and $0.01 \leqslant Ra^* \leqslant 100$. The problem under such conditions is rarely investigated. This has motivated the present investigation.

2. ANALYSIS

The physical situation and coordinate system are shown in Fig. 1. The projection of the enclosure is of a vertical rectangular cross-section, with hot isothermal top and circumferential surfaces (T_h) and with the bottom wall kept at a lower temperature (T_c). The flow is assumed to be two-dimensional. The fluid in the porous enclosure is assumed to have constant properties except insofar as the buoyancy is concerned; the convecting fluid and the porous matrix are in local thermodynamic equilibrium; Darcy's law and the Boussinesq approximations are employed.

Then, the equations that account for the conservation of mass, momentum, and energy for the porous enclosure are as follows:

NOMENCLATURE

g	gravitational acceleration	β	thermal expansion coefficient
h	height of the porous cavity	λ	anisotropic thermal conductivity ratio
H	height of the enclosure	θ	dimensionless temperature, $(T-T_c)/(T_h-T_c)$
k	thermal conductivity	μ	viscosity of fluid
K	permeability	ρ	density of fluid.
K^*	anisotropic permeability ratio		
Nu	local Nusselt number		
P'	pressure	Superscript	
P	dimensionless pressure	$\bar{}$	average quantities.
Ra^*	Darcy modified Rayleigh number		
T	temperature	Subscripts	
U, V	dimensionless velocity in r, z directions	b	bottom wall
r, z	radial and vertical coordinates	c	cold
R, Z	dimensionless coordinates.	h	hot
		s	side wall
Greek symbols		t	top wall
α_r	thermal diffusivity in r-direction	r	r-direction
α_z	thermal diffusivity in z-direction	z	z-direction.

$$\frac{\partial}{\partial r}(rV_r)+\frac{\partial}{\partial z}(rV_z)=0 \tag{1}$$

$$V_r=-\frac{K_r}{\mu}\frac{\partial P'}{\partial r} \tag{2}$$

$$V_z=-\frac{K_z}{\mu}\left[\frac{\partial P'}{\partial z}-\rho g\beta(T-T_c)\right] \tag{3}$$

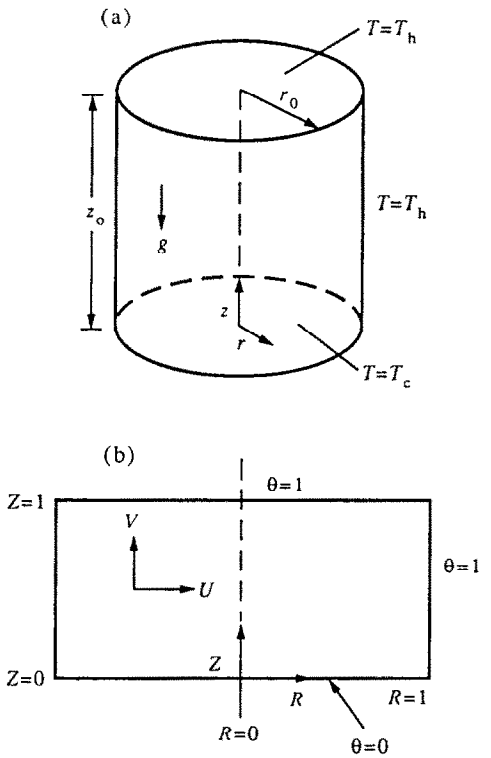

FIG. 1. Schematic of the physical system.

$$\rho C\left(V_r\frac{\partial T}{\partial r}+V_z\frac{\partial T}{\partial z}\right)=k_r\left[\frac{1}{r}\frac{\partial}{\partial r}\left(r\frac{\partial T}{\partial r}\right)\right]+k_z\frac{\partial^2 T}{\partial Z^2} \tag{4}$$

with boundary conditions:

$$\begin{aligned} &r=0: && \frac{\partial V_r}{\partial r}=0, && \frac{\partial T}{\partial r}=0\\ &r=r_0: && V_r=0, && T=T_h\\ &z=0: && V_z=0, && T=T_c\\ &z=z_0: && V_z=0, && T=T_h \end{aligned} \tag{5}$$

where K_r and K_z are the r- and z-direction permeability of the saturated porous medium, respectively; k_r and k_z are the r-direction and z-direction thermal conductivity, respectively. The other various symbols are defined in the Nomenclature.

The following dimensionless variables are introduced:

$$R=\frac{r}{r_0},\quad Z=\frac{z}{z_0},\quad K^*=\frac{K_r}{K_z},\quad \lambda=\frac{k_r}{k_z},\quad \alpha_r=\frac{k_r}{\rho c}$$

$$\alpha_z=\frac{k_z}{\rho c},\quad U=\frac{V_r r_0}{\alpha_r},\quad V=\frac{V_z r_0}{\alpha_r},\quad A=\frac{Z_0}{r_0}$$

$$P=\frac{P'K_r}{\alpha_r\mu},\quad \theta=\frac{T-T_c}{T_h-T_c},\quad Ra^*=\frac{K_r g\beta r_0(T_h-T_c)}{\alpha_r\nu}. \tag{6}$$

Then, equations (1)–(4) become

$$\frac{\partial U}{\partial R}+\frac{U}{R}+\frac{1}{A}\frac{\partial V}{\partial Z}=0 \tag{7}$$

$$U=-\frac{\partial P}{\partial R} \tag{8}$$

$$V = -\frac{1}{K^* A}\frac{\partial P}{\partial Z} + \frac{1}{K^*} Ra^* \cdot \theta \tag{9}$$

$$U\frac{\partial \theta}{\partial R} + \frac{1}{A} V \frac{\partial \theta}{\partial Z} = \frac{\partial^2 \theta}{\partial R^2} + \frac{1}{R}\frac{\partial \theta}{\partial R} + \frac{1}{\lambda A^2}\frac{\partial^2 \theta}{\partial Z^2} \tag{10}$$

with the dimensionless boundary conditions

$$\begin{aligned} &R = 0; \quad \frac{\partial U}{\partial R}, \ \frac{\partial \theta}{\partial R} = 0 \\ &R = 1; \quad U = 0, \quad \theta = 1 \\ &Z = 0; \quad V = 0, \quad \theta = 0 \\ &Z = 1; \quad V = 0, \quad \theta = 1. \end{aligned} \tag{11}$$

When $K^* = \lambda = 1$, equations (7)–(11) are reduced to the traditional problem of isotropic porous media with isotropic thermal diffusivity.

In terms of new variables, it can be shown that the local and average Nusselt numbers are given by

$$Nu_b = \frac{\partial \theta}{\partial Z} \quad \text{at} \quad Z = 0$$

$$Nu_t = \frac{\partial \theta}{\partial Z} \quad \text{at} \quad Z = 1$$

$$Nu_s = \frac{\partial \theta}{\partial R} \quad \text{at} \quad R = 1$$

and

$$\begin{aligned} \overline{Nu_b} &= 2\int_0^1 R \frac{\partial \theta}{\partial Z}\bigg|_{Z=0} \\ \overline{Nu_s} &= \int_0^1 \frac{\partial \theta}{\partial R}\bigg|_{R=1} \mathrm{d}z \\ \overline{Nu_t} &= 2\int_0^1 R \frac{\partial \theta}{\partial Z}\bigg|_{Z=1} \mathrm{d}r \end{aligned} \tag{12}$$

where the Nu_b, Nu_t and Nu_s are the local Nusselt numbers for the bottom, top and sidewall, respectively.

3. NUMERICAL METHOD OF SOLUTION

The numerical procedure used is based on the iterative scheme. The hybrid central/upwind differences is used for the convective terms with central difference for the diffusion terms. For the convective term, upwind differencing is used if the grid Peclet number in a given direction is greater than or equal to 2, while central differences are employed when grid $Pe < 2$. This procedure is incorporated into the SIMPLE solution technique initiated by Patankar [20]. The set of difference equations is solved over the entire region of interest by obtaining new values for any desired variable by taking into account the latest-known estimated value of that variable on the neighboring nodes. One iteration of the solution is completed when, in a line-by-line technique, all the lines in a chosen direction have been accounted for. Line inversion iteration with an under relaxation value of 0.5 for velocity terms, 0.6 for the pressure correction term and 0.8 for the temperature term was incorporated to facilitate calculation.

A convectional numerical scheme with nonuniform (31×31) grids, was applied to the present physical system. The finest grid, of size 0.01, are located adjacent to the wall and the centerline, and the size of other grids is chosen such that each is within 110% of its neighboring grids in order to avoid abrupt changes and divergence.

By first assuming a pressure distribution within the pressure cavity domain, the set of difference equations for the r- and z-momentum and energy equations is solved for the porous cylinder. After a sweep of the solution domain is completed, adjustments are made to the pressure field so that the continuity, momentum, and energy equations are satisfied simultaneously. The convergence criterion adopted is that the change of variable at any node should be less than 0.0001.

The adequacy of the grid is verified by comparing the results computed with a 31×31 grid with those obtained using a 61×61 grid. The comparison for the temperature distributions at different radial and elevation is agreed. For example, the maximum discrepancy between the temperature distributions for the two grid sizes is within 0.0001 and the average Nusselt numbers along all surfaces agree to the third significant digit beyond the decimal point.

4. RESULTS AND DISCUSSIONS

Numerical results for the streamlines, isotherms and the Nusselt number are obtained for $0.1 \leqslant K^* \leqslant 10$, $0.1 \leqslant \lambda \leqslant 10$, $0.5 \leqslant A \leqslant 2$ and $0.01 \leqslant Ra^* \leqslant 100$.

Figure 2 shows the effects of anisotropic permeability on the streamlines and isothermal lines. From Fig. 2(b) ($K^* = 1$; i.e. isotropic porous media), the flow is clearly driven by the temperature difference between the bottom wall and the circumferential and top surfaces. The heated top wall and vertical sidewall as well as the cooled bottom wall are lined by boundary layers. The vertical boundary layer is most evident in the lower section of height, where it is sandwiched by the most pronounced temperature difference ΔT. Above this height the vertical jet accelerated in the vertical boundary-layer region discharges into a pool of the nearly isothermal trapped fluid. The vertical jet decelerates and loses much of its momentum before smoothly rounding the upper right-hand corner of the enclosure. In addition, the eye of the vortex approaches the lower right-hand corner. Figures 2(a)–(c) indicate that as K^* increases from 0.1 to 10, the vortex is more inclined to the bottom wall, and the high temperature region becomes smaller. Therefore, the top wall heat transfer rate increases with increasing the values of K^*.

Figure 3 shows the variation of the average Nusselt number of the bottom side with K^* at four different

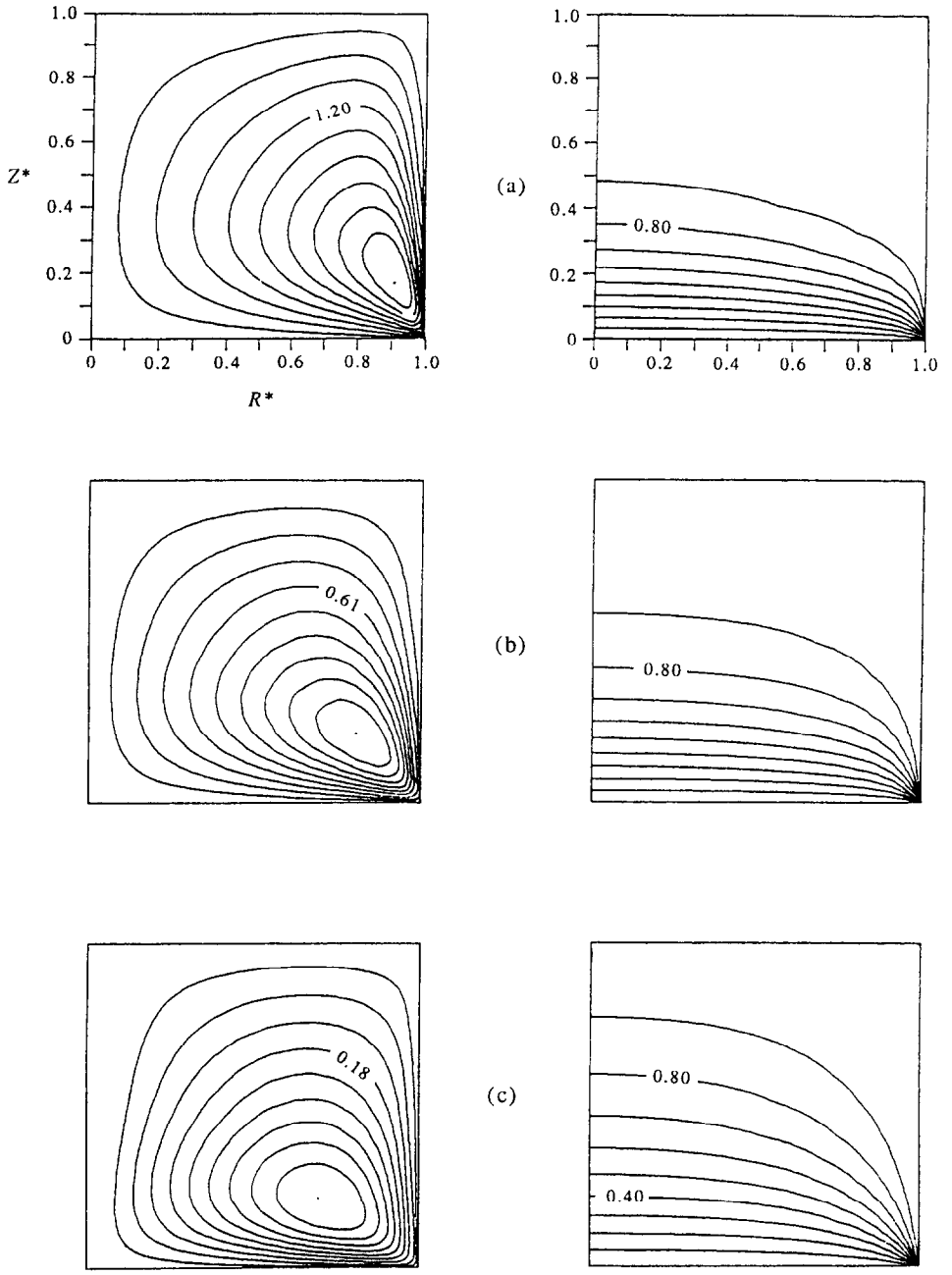

FIG. 2. The streamlines and isotherms patterns for $A = 1$, $Ra^* = 100$, $\lambda = 1$, (a) $K^* = 0.1$, (b) $K^* = 1$, (c) $K^* = 10$.

values of Ra^*. It is shown that as the value of K^* increases, the average Nusselt number decreases. This characteristic becomes more visible as Ra^* increases. It is also indicated that as Ra^* increases, the average Nusselt number increases. Figure 4 shows the variation of the average Nusselt number of the sidewall with K^* for different values of Ra^*. It is shown that the phenomenon is similar to Fig. 3. However, these phenomena are not observed at the top side. Figure 5 shows that the average Nusselt number of the top side increases with increasing the value of K^* or decreasing the value of Ra^*. From Figs. 3–5, it is found that a major fraction of the total heat transfer occurs from the lower sidewall, while the top wall seems to be insulated in all cases.

The local Nusselt number distributions on the sidewall along the cylindrical axis are plotted in Fig. 6 for three different values of aspect ratio A. The local Nusselt number decreases monotonically as Z increases to the top wall, and the heat transfer is most

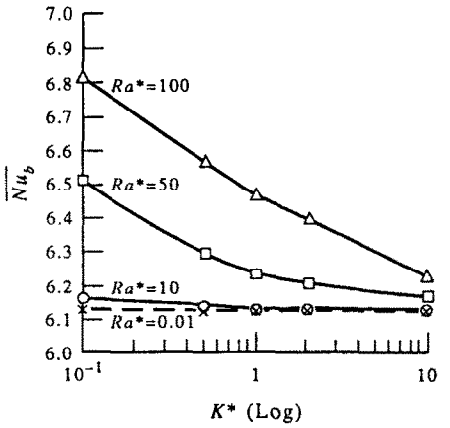

FIG. 3. The variation of the average Nusselt number of the bottom wall with K^* for different Ra^* at $A = 1$, $\lambda = 1$.

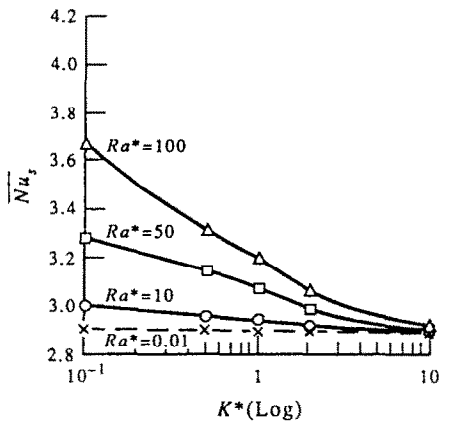

FIG. 4. The variation of the average Nusselt number of the sidewall with K^* for different Ra^* at $A = 1$, $\lambda = 1$.

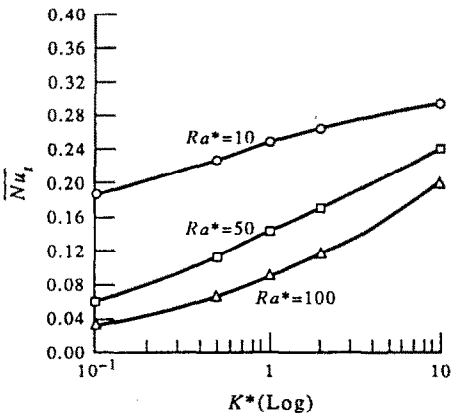

FIG. 5. The variation of the average Nusselt number of the top wall with K^* for different Ra^* at $A = 1$, $\lambda = 1$.

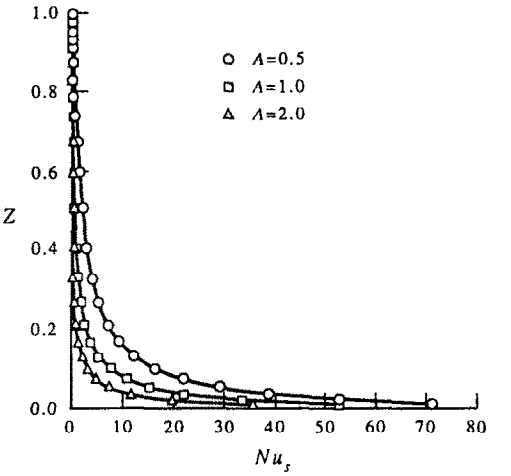

FIG. 6. The variation of the local Nusselt number of the side wall with Z for different aspect ratio ($K^* = 1$, $\lambda = 1$, $Ra^* = 50$).

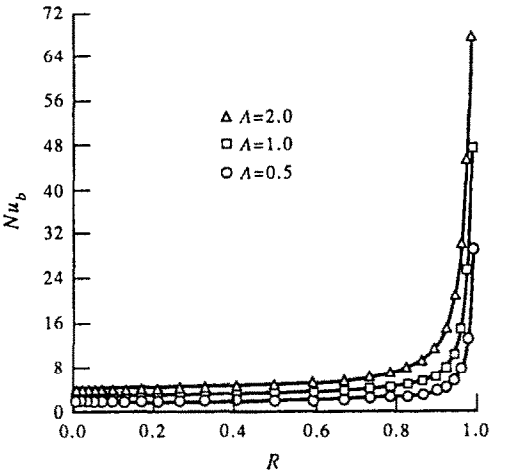

FIG. 7. The variation of the local Nusselt number of the bottom wall with R for different aspect ratio ($K^* = 1$, $\lambda = 1$, $Ra^* = 50$).

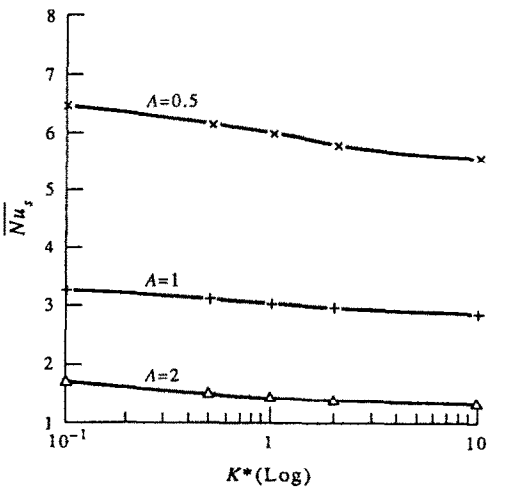

FIG. 8. The variation of the average Nusselt number of the side wall with K^* for different aspect ratio ($Ra^* = 50$, $\lambda = 1$).

evident in the lower section of height, which decreases with increasing the aspect ratio A. Figure 7 shows the variation of the local Nusselt number on the bottom wall with R. It is seen that the primary heat transfer occurs nearby at $R = 1$, and when aspect ratio A decreases, the primary heat transfer occurs more nearby at $R = 1$. Figure 8 shows the variations of the $\overline{Nu}_s$ vs K^* for three different values of A. It is shown that as aspect ratio A increases two times, the $\overline{Nu}_s$ decreases to half of the original values. It is also indicated that $\overline{Nu}_s$ decreases with increasing the values of K^*.

The effects of anisotropic thermal conductivity ratio on the streamlines and isothermal lines are shown in Fig. 9. It is seen that as λ increases, the eye of the vortex approaches toward the lower right-hand corner and also inclines towards the bottom wall. In addition, the high temperature region becomes larger as λ increases. The variations of the Nusselt number with anisotropic permeability and thermal conductivity ratio for the bottom and side wall are shown in Figs. 10 and 11, respectively. As expected, both the $\overline{Nu}_b$ and $\lambda \cdot \overline{Nu}_s$ increase as λ increases.

5. CONCLUSION

The numerical solutions have shown significant effects of anisotropic permeabilities, thermal conductivities on the convective heat transfer in a vertical cylindrical porous media. The major fraction of the

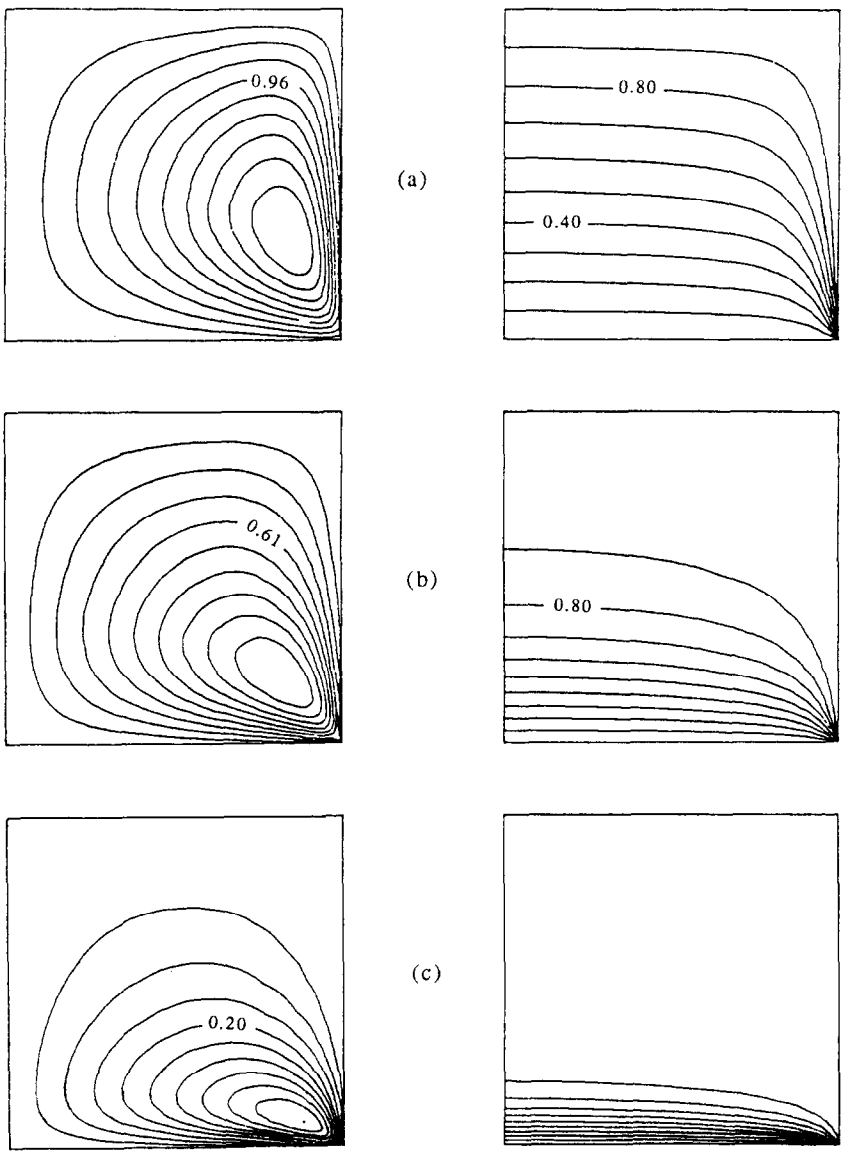

FIG. 9. The streamlines and isotherms patterns for $A = 1$, $Ra^* = 50$, $K^* = 1$, (a) $\lambda = 0.1$, (b) $\lambda = 1$, (c) $\lambda = 10$.

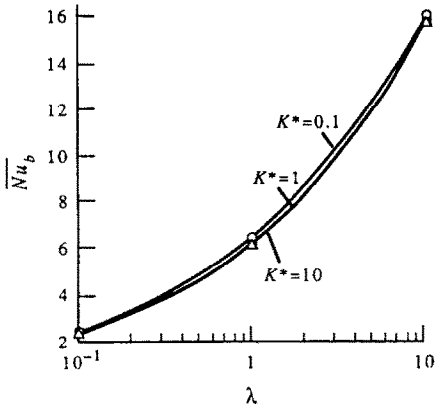

FIG. 10. The variation of the Nusselt number of the bottom wall with λ and K^* ($Ra^* = 50$, $A = 1$).

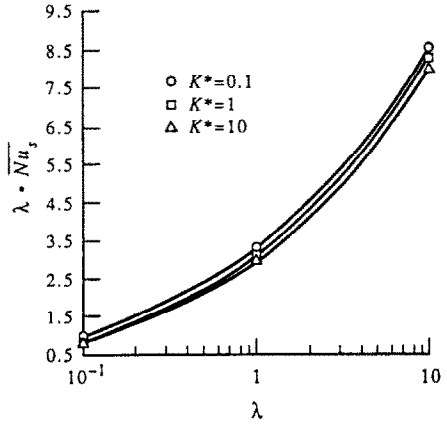

FIG. 11. The variation of the Nusselt number of the side wall with λ and K^* ($Ra^* = 50$, $A = 1$).

total heat transfer comes from the lower side wall, while the top wall seems to be insulated in all cases we analyzed. The heat transfer is more evident in the lower section of height as the aspect ratio A decreases. The vortex is more inclined to the bottom wall, and the high temperature region becomes smaller as K^* increases. The eye of the vortex approaches toward the lower right-hand corner, also inclines toward the bottom wall and the high temperature region enlarges as k increases. The heat transfer rate of the side wall and bottom wall increases, either decreasing the values of anisotropic permeability ratio or increasing the values of anisotropic thermal conductivities ratio.

REFERENCES

1. P. Cheng, Heat transfer in geothermal system, *Adv. Heat Transfer* **14**, 1–105 (1978).
2. P. Cheng, Natural convection in a porous medium: external flows, *NATO Advanced Study Institute on Natural Convection: Fundamentals and Applications*, Izmir, Turkey, 16–27 July (1984).
3. M. A. Combarnous, Natural convection in porous medium and geothermal system, *Proceedings of the 6th International Heat Transfer Conference*, Vol. 6, pp. 45–59 (1978).
4. K. J. Schneider, Investigation of the influence of free thermal convection on heat transfer through granular material, *Int. Inst. Refrigeration Proceedings*, pp. 247–253 (1963).
5. J. W. Weber, The boundary layer regime for convection in a vertical porous layer, *Int. J. Heat Mass Transfer* **18**, 569–573 (1975).
6. A. Bejan, On the boundary layer regime for convection in a vertical enclosure filled with a porous medium, *Lett. Heat Mass Transfer* **6**, 93–102 (1979).
7. M. B. Peirotti, M. D. Giavedoni and J. A. Deiber, Natural convective heat transfer in a rectangular porous cavity with variable fluid properties validity of the Boussinesq approximation, *Int. J. Heat Mass Transfer* **30**, 2571–2581 (1987).
8. P. Vasseur, M. G. Satih and L. Robillard, Natural convection in the thin, inclined, porous, layer, exposed to a constant heat flux, *Int. J. Heat Mass Transfer* **30**, 537–549 (1987).
9. D. Poulikakos and A. Bejan, Natural convection in a porous layer heated and cooled along one vertical side, *Int. J. Heat Mass Transfer* **27**, 1879–1891 (1984).
10. V. Prasad and F. A. Kulacki, Convective heat transfer in a rectangular porous cavity effect of aspect ratio on flow structure and heat transfer, *ASME J. Heat Transfer* **106**, 158–165 (1984).
11. V. Prasad and F. A. Kulacki, Natural convection in a rectangular porous cavity with constant heat flux on one vertical wall, *ASME J. Heat Transfer* **106**, 152–157 (1984).
12. C. W. Horton and F. T. Rogers, Convection currents in a porous medium, *J. Appl. Phys.* **16**, 367 (1945).
13. R. A. Wooding, Steady state free convection of a liquid in a saturated permeable medium, *J. Fluid Mech.* **2**, 273–285 (1957).
14. R. N. Horne and M. J. O'Sullivan, Oscillatory convection in a porous medium heated from below, *J. Fluid Mech.* **66**, 339–352 (1974).
15. M. A. Combarnous et B. LeFur, Transfert de Chaleur par Convection Naturelle dans une Couche Poreuse Horizontale, *Comptes Rendus Academie Sciences Paris* **t.269**, Series B, 1009–1012 (1969).
16. J. P. Caltagirone, M. Cloupeau and M. A. Combarnous, Fluctuating natural convection in a porous horizontal layer, *Comptes Rendus Academie Sciences Paris* **t.273**, Series B, 833–836 (1971).
17. O. Kvernvold and P. A. Tyvand, Nonlinear thermal convection in anisotropic porous media, *J. Fluid Mech.* **90**, 609–624 (1979).
18. P. J. Burns, L. C. Chow and C. L. Tien, Convection in a vertical slot filled with porous insulation, *Int. J. Heat Mass Transfer* **20**, 919–926 (1977).
19. S. Bories, Natural convection in porous media, *Advances in Transport Phenomena in Porous Media*, NATO ASI Series. Nijhoff, Dordrecht (1987).
20. S. V. Patankar, *Numerical Heat Transfer and Fluid Flow*. Hemisphere, Washington, D.C. (1980).